

Performance outlook of the SCRAP receiver

Matti Lubkoll, Theodor W. von Backström, and Thomas M. Harms

Citation: [AIP Conference Proceedings](#) **1734**, 030024 (2016); doi: 10.1063/1.4949076

View online: <http://dx.doi.org/10.1063/1.4949076>

View Table of Contents: <http://scitation.aip.org/content/aip/proceeding/aipcp/1734?ver=pdfcov>

Published by the [AIP Publishing](#)

Articles you may be interested in

[Optimization of acoustic receiver noise performance](#)

J. Acoust. Soc. Am. **61**, 1471 (1977); 10.1121/1.381464

[Comparison of Receiver Performance: the ESP Receiver](#)

J. Acoust. Soc. Am. **45**, 233 (1969); 10.1121/1.1911362

[Evaluation of the Performance of Active Sonar Receivers](#)

J. Acoust. Soc. Am. **41**, 767 (1967); 10.1121/1.1910404

[SCRAPS: Numbers](#)

Phys. Teach. **1**, 46 (1963); 10.1119/1.2350571

[Performance of Telephone Receivers as Affected by the Ear](#)

J. Acoust. Soc. Am. **6**, 250 (1935); 10.1121/1.1915744

Performance Outlook of the SCRAP Receiver

Matti Lubkoll^{1,a)}, Theodor W. von Backström¹ and Thomas M. Harms¹

¹*Solar Thermal Energy Research Group, Stellenbosch University, Private Bag XI, Matieland 7602, Stellenbosch, South Africa*

^{a)}Corresponding author: matti@sun.ac.za

Abstract. A combined cycle (CC) concentrating solar power (CSP) plant provides significant potential to achieve an efficiency increase and an electricity cost reduction compared to current single-cycle plants. A CC CSP system requires a receiver technology capable of effectively transferring heat from concentrated solar irradiation to a pressurized air stream of a gas turbine. The small number of pressurized air receivers demonstrated to date have practical limitations, when operating at high temperatures and pressures. As yet, a robust, scalable and efficient system has to be developed and commercialized.

A novel receiver system, the Spiky Central Receiver Air Pre-heater (SCRAP) concept has been proposed to comply with these requirements. The SCRAP system is conceived as a solution for an efficient and robust pressurized air receiver that could be implemented in CC CSP concepts or standalone solar Brayton cycles without a bottoming Rankine cycle.

The presented work expands on previous publications on the thermal modeling of the receiver system. Based on the analysis of a single heat transfer element (spike), predictions for its thermal performance can be made. To this end the existing thermal model was improved by heat transfer characteristics for the jet impingement region of the spike tip as well as heat transfer models simulating the interaction with ambient. While the jet impingement cooling effect was simulated employing a commercial CFD code, the ambient heat transfer model was based on simplifying assumptions in order to employ empirical and analytical equations.

The thermal efficiency of a spike under design conditions (flux 1.0 MW/m^2 , air outlet temperature just below $800 \text{ }^\circ\text{C}$) was calculated at approximately 80%, where convective heat losses account for 16.2% of the absorbed radiation and radiative heat losses for a lower 2.9%. This effect is due to peak surface temperatures occurring at the root of the spikes. It can thus be concluded that the geometric receiver layout assists to limit radiative heat losses.

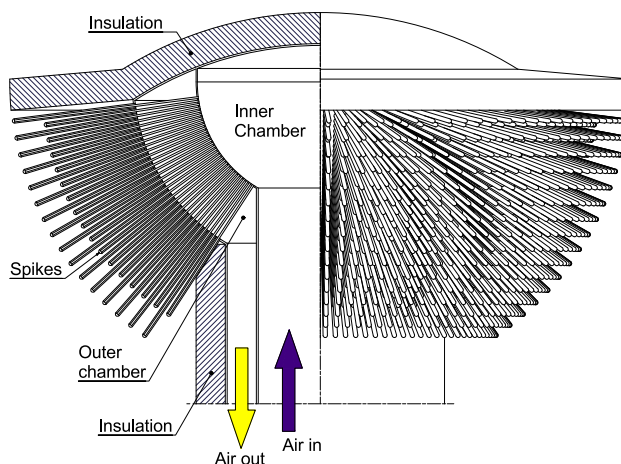


FIGURE 1: A manifestation of the SCRAP receiver (left half in section) [3]

INTRODUCTION

Pressurized air receivers are a young field of research with a small amount of receivers proposed and tested to date. It was found that a solar receiver system that provides good solar-thermal efficiency, good optical efficiency (not requiring a CPC and operating on a surrounding heliostat field), is robust (not dependent of fragile materials) and operates under a low pressure drop has yet to be found [1].

The SCRAP receiver was conceived with the intention to overcome these challenges in an effective, robust and cost-efficient manner. The SCRAP receiver is intended as an external metallic tubular pressurized air receiver, with purpose of pre-heating an air stream to up to 800 °C upstream of a gas turbine's combustion chamber (or secondary receiver) [2].

The Receiver Concept

A manifestation of the receiver is shown in Figure 1. The tubular absorber assemblies (referred to as spikes) are concentrically arranged in a way that they describe a body of increasing density towards the receiver center and allow for a receiver type that can operate with a surrounding heliostat field, leading to increased annual optical solar field efficiency.

The 'cold' air (e.g. from a compressor stage) enters the receiver through an inner chamber. From there the air stream is directed through a multitude of circular tubes into the absorber assemblies. Each spike (see Figure 2) consists of two concentric tubes, where the inner tube supplies the cold air stream from the inner chamber to the spike tip (outermost point) from where the air flow is directed back by 180° towards the receiver center, passing through the outer tube. The outer tube's outer surface is exposed to the concentrated irradiation, and in the process heated up, transferring thermal energy to the pressurized air stream.

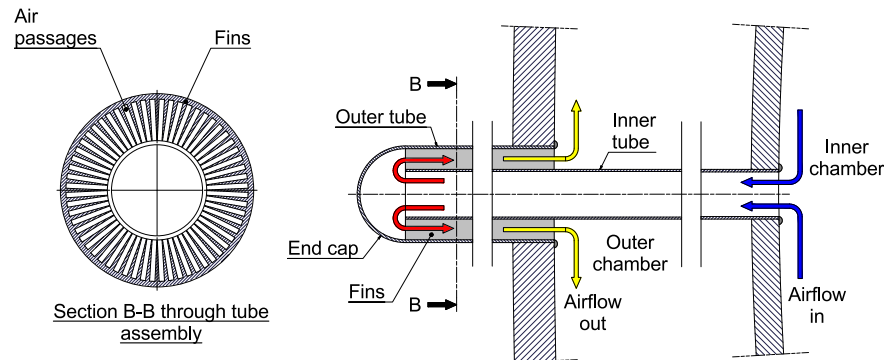


FIGURE 2: Conceptual geometry of the internally finned tube [3]

The temperature of the outer tube wall is intended to rise from the spike tip towards the highest temperature at the spike root (where it is mounted to the receiver structure). With radiative heat losses gaining significance at higher temperatures this spike surface temperature distribution becomes advantageous. As a result a macro-volumetric effect is envisaged, where high material temperatures occur deep within the receiver. A high cooling effect is achieved at the most exposed area, the spike tip, where relatively cool air exits the inner tube. With lower solar irradiation expected towards the spike root, the risk of absorber pipe overheating is lowered.

Previous Work

A ray-tracing study was conducted in order to understand the receiver's sensitivity to solar field parameters. It was found that the effect of heliostat size/facet size has a notable effect on the flux distribution along a spike [2]. As the spike tip points towards the solar field it experiences the highest flux. Due to the geometry of the spike tip a strong cooling effect of the impinging air stream onto the tip surface (end cap in Figure 2) - as it changes the flow direction by 180° - is envisaged. The heat transfer model introduced in [2] describes the internal heat transfer within a spike. In the model the spike tip is treated as a black box requiring an averaged Nusselt number (Nu) and flux input. This study expands that model by providing results on an analysis of jet impingement cooling of the spike tip.

Further, to enable predictions of the performance of a spike, models for convective and radiative heat loss to ambient are introduced. This allows to gain understanding of the thermal interaction between spikes.

HEAT TRANSFER MODEL

A simplified heat transfer model was introduced in [2]. The flow model is meshed linearly, however, due to the return flow configuration, thermal interaction occurs between upstream and downstream nodes far apart (e.g. a cell near the outlet of a rectangular duct heats the in-flowing ‘cold’ air from the inner chamber through the inner tube). Two models, one for jet impingement cooling, and one for thermal interaction with ambient are presented in the following.

Impingement Cooling

As shown later the tip performance is not of dominant nature for the thermal performance of the entire spike. An error of 10 % in heat loss prediction from the tip would result in a total heat loss error of about 1.5 %. With treating the tip as a single cell, wall surface dimension, inlet flow parameters, solar flux and wall temperature as well as the Nusselt number are averaged. A well designed and optimized spike tip aiming at maximized thermal performance at minimal pressure drop bears complexity and challenges to justify an individual research project.

Impinging jets can generate a peak Nusselt number in the center point of the flow impingement on a surface. In the case of a spike that occurs at the same area that experiences peak solar flux as it points directly into the heliostat field. The flux reduces along the tip surface. With that in mind it is found sufficient to initially supply the program with averaged information, as naturally the jet tends to cool the strongest, where the flux is the highest.

The commercial CFD software ANSYS® FLUENT (Release 15.0) was used as a simulation tool to analyze the jet impingement effects. As noted, with the goal of averaged information it was understood that CFD models may vary notably from measured results [4]. With that in mind it was decided to initially limit the simulations to using the $k-\varepsilon$ model and the Reynolds-Stress-Model (RSM). Should need arise further models such as the $\nu^2 f$ model can be considered.

An axis symmetric two-dimensional model was reproduced where a pipe of diameter D points a jet at a heated plate a distance H/D from the nozzle. A scenario with a Reynolds number of $Re = 23\,000$ and $H/D = 6$ was simulated and compared to experimental data. Curves for the standard $k-\varepsilon$ model, the realizable $k-\varepsilon$ model as well as the RSM are shown in Figure 3.

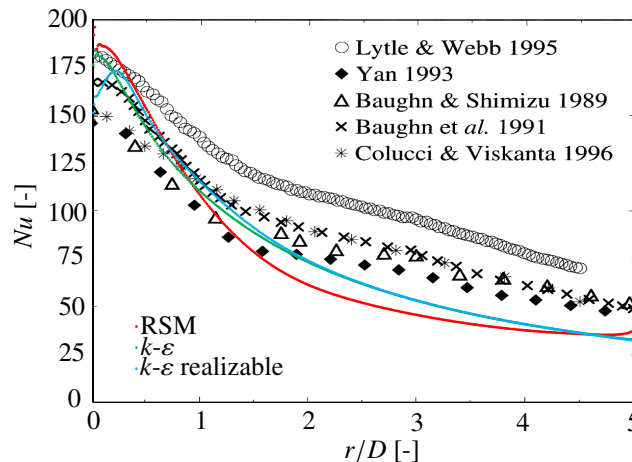


FIGURE 3: Nu over r/D for $k-\varepsilon$ model, realizable $k-\varepsilon$ model as well as RSM model over various experimental results (simulation results overlaid on experimental results summarized by [5])

Here, the Nusselt number is defined as $Nu = h D/k$, where D is the pipe diameter, k the air’s thermal conductivity at pipe outlet and h the local heat transfer coefficient computed from the local heat flux with reference to the mean pipe outlet temperature. All three models appear to predict peak Nu rather well in the stagnation zone near $r/D = 0$. The realizable $k-\varepsilon$ model does not result in more accurate predictions than the standard $k-\varepsilon$ model and predicts a dip

in the center of the stagnation zone that is not expected from studying the experimental data [5]. Towards larger r/D values the three models under-predict the local Nusselt numbers. This effect is less pronounced for the $k-\varepsilon$ models as compared to the RSM model. It appears that the $k-\varepsilon$ model can generate results in a sufficiently accurate range for the purpose of the analysis with a tendency to under-predict rather than over-predict.

The $k-\varepsilon$ model provided reasonable results at low computational expense compared to the RSM. Further investigations were as a consequence conducted based on the $k-\varepsilon$ model. To predict impingement cooling on a spike tip, studies were done on an annular surface, omitting the fins in the outer tube section. As a result 2-d meshes were used. Figure 4 shows the Nusselt number over a section of the tip surface over a range of Reynolds numbers. The mass flow rate for each case is constant and higher Re are result of nozzle diameters smaller than the standard inner tube diameter. Here, differing nozzle sizes are simulated by using according tube diameters in order to generate reproducible fully developed flow profiles.

The angle ϕ is measured from the spike axis and has an angle of 0° at the tip and perpendicular to it at 90° , where the tip region exits into the out tube section. It has to be noted that by holding the mass flow rate \dot{m} constant, the Reynolds number increases for smaller nozzle sizes. Equally does the value of H/D increase for smaller nozzle sizes as the outlet point is kept at the same location. It can be seen that the stagnation zone for solutions based on large pipe diameters D (and thus low H/D) reaches a size large enough to have a sizable negative impact on heat being transported away by the air stream in a meaningful quantity. This occurrence is observed in Figure 4, where Nu drops towards the spike tip ($\phi = 0^\circ$).

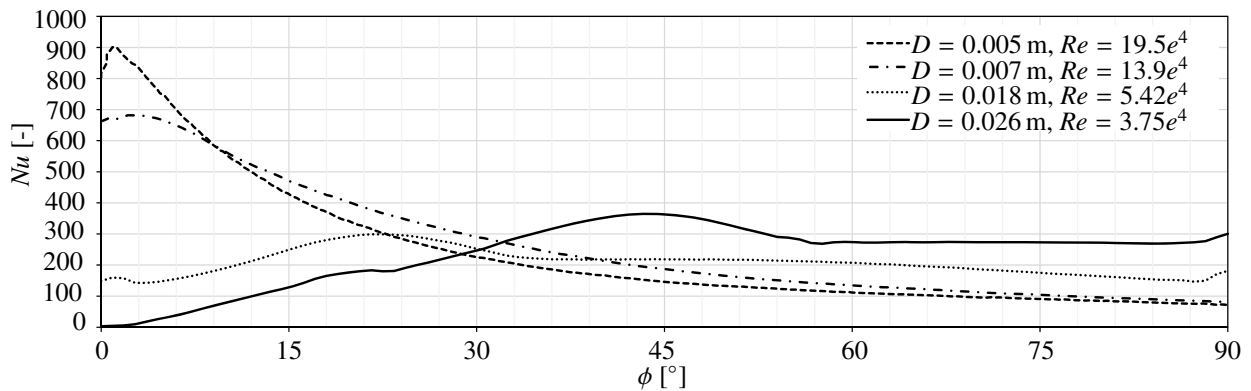


FIGURE 4: Nu over ϕ , using the $k-\varepsilon$ model for nozzle sizes from 5 mm to 26 mm; $\phi = 0$ is in axial spike direction (data for an air stream at 9.8 m/s, 540 °C, 10 bar)

Noting that $h = Nu k/D$ it becomes apparent to what extend acceleration of the air stream by smaller nozzle diameters can lead to heat transfer enhancements. Having the annular section replaced with rectangular ducts and fins as illustrated in Figure 2 is expected to somewhat increase Nu as the flow is prevented from decelerating as much as with a large annular space.

Work is needed on designing this section with particular attention towards the resulting pressure drop. For the current state of the project it is sufficient to be able to make use of adequate Nusselt numbers. The way the air stream behaves within the tip and downstream of the tip depends significantly on the nozzle design and position. Until a optimized model of a spike tip is employed, convective heat transfer in downstream nodes is calculated based on the fully developed flow and temperature profiles. Pressure drop inflicted by the nozzle and the jet impingement are supplied to the code via the tip node. This includes further downstream pressure drop resulting from the air stream entering the rectangular ducts and developing. Pressure drop analysis, however, not part of this study as meaningful results considering the application require a more global systems analysis.

Interaction with Ambient

To establish a first understanding of system performance to be expected, thermal interaction with ambient was added to the heat transfer model. Convective heat transfer as well as radiative heat transfer models are outlined below.

Convective Heat Loss

The convective heat transfer to ambient was simulated using a combined heat transfer coefficient for natural convection as well as forced convection

$$h_{\text{combined}} = (h_{\text{forced}}^n + h_{\text{natural}}^n)^{1/n}, \quad (1)$$

where n in the blending parameter. [6] recommend $3 \leq n \leq 4$. A smaller blending parameter leads to increased influence of the smaller heat transfer mechanism, typically the natural convection. A blending parameter of 3.2 has been used by Garbrecht *et al.* [7], which has been proposed for cavity receivers. $n = 3$ serves as a conservative approach, further used in this model.

The forced convection heat transfer coefficient over the spike is computed by Churchill and Bernstein's equation

$$h_{\text{forced, cylinder}} = \frac{k}{D} \left(0.3 + \frac{0.62Re^{1/2}Pr^{1/3}}{[1 + (0.4/Pr)^{2/3}]^{1/4}} \left[1 + \left(\frac{Re}{280000} \right)^{5/8} \right]^{4/5} \right), \quad (2)$$

where the air parameters are computed at the film temperature $T_{\text{film}} = (T_{\text{wind},\infty} + T_s)/2$. The heat transfer coefficient of the tip is approximated with h for a spherical shape, using Whitaker's equation:

$$h_{\text{forced, sphere}} = \frac{k}{D} \left(2 + [0.4Re^{1/2} + 0.06Re^{2/3}] Pr^{0.4} \left(\frac{\mu_{\infty}}{\mu_s} \right)^{1/4} \right), \quad (3)$$

where the air properties are computed at free stream temperature (except the viscosity μ_s , which is computed at the surface temperature T_s).

Natural convection heat transfer coefficients are based on empirical correlations provided in [6]:

$$h_{\text{natural, cylinder}} = \frac{k}{D} \left(0.6 + \frac{0.387Ra^{1/6}}{[1 + (0.559/Pr)^{9/16}]^{8/27}} \right)^2, \quad (4)$$

and

$$h_{\text{natural, sphere}} = \frac{k}{D} \left(2 + \frac{0.589Ra^{1/4}}{[1 + (0.469/Pr)^{9/16}]^{4/9}} \right), \quad (5)$$

where in both equations the fluid properties are based on the film temperature.

Radiative Heat Loss

Each spike interacts through thermal radiation not only with ambient but also with neighboring spikes. To compute radiative heat transfer the view factor $F_{1 \rightarrow 2}$ between interacting bodies 1 and 2 is required

$$\dot{q}_{\text{rad},1 \rightarrow 2}'' = \sigma F_{1 \rightarrow 2} \epsilon_1 (T_{s,1}^4 - T_{s,2}^4). \quad (6)$$

As illustrated earlier, the spike is incremented in axial direction, resulting in cylindrical outer surface elements. To make use of readily available equations to compute the view factors, the geometry surrounding the investigated spike requires simplification.

The neighboring spikes are represented by a frustum shape positioned through their axis (see Figure 5 left). Note that Figure 5 serves illustrative purpose and is not to scale. View factor equations are available for interaction of a cylindrical object inside a frustum [8]. The frustum is axially incremented in equal resolution to the spike to enable thermal interaction with neighboring spikes under the assumption of these operating under identical conditions.

The view factor of each outer cylindrical element of the spike is also computed to ambient (as a disc closing the frustum to the outside, see Figure 5) as well as to the receiver's outer chamber's surface at the spike root (equally computed as view factor to a disc). Equations for view factors from a cylindrical surface to a disc are also available in literature [8].

Between the different spikes first order radiative heat transfer is considered and further reflection thereof neglected.

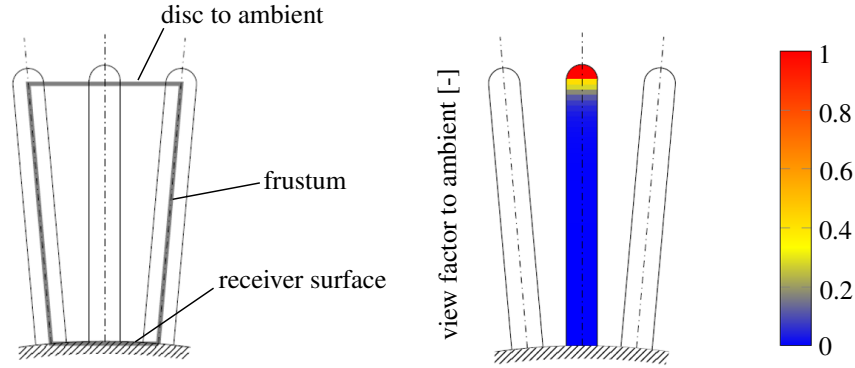


FIGURE 5: Illustration of the frustum representing neighboring spikes for computation of view factors $F_{1 \rightarrow 2}$ (left) and view factors to ambient for a given setup (right)

RESULTS AND INTERPRETATION

A simulation of a spike was conducted including thermal interaction with ambient. The simulation was set to provide an air outlet temperature of approximately 800 °C. Relevant input data is listed in Table 1. Air properties as well as metal properties were modeled as temperature dependent. The ambient wind velocity was assumed with a quadratic equation with $u = 0$ m/s at the spike root and $u = u_{\text{wind}\infty}$ at the tip.

TABLE 1: Simulation input data

Parameter	Unit	Value
$r_{\text{outer chamber}}$	m	2
L_{spike}	m	1.3
D_{spike}	m	0.07
n_{ducts}	–	24
$Nu_{\text{tip, mean}}$	–	150
p_{inlet}	bar	10
T_{inlet}	°C	300
u_{inlet}	m/s	8.05
\dot{q}_{rad}	MW/m ²	1.0
n	–	3
$u_{\text{wind},\infty}$	m/s	3.0

The simulation converged at an air outlet temperature of 792 °C. The peak metal temperature was experienced at the root of the spike with 866 °C as compared to the tip at 664 °C. The radiative and convective heat losses to ambient are shown in Figure 6.

It was found that the total convective heat loss dominates the overall radiative heat loss. The view factor to ambient, as seen in Figure 5, drops to insignificant magnitude quickly as the distance to the tip grows. On the other hand the assumption that wind would be of a quadratic profile along the spike (zero velocity at root) is responsible for high convective losses towards the tip. Towards the root of the spike natural convection results in notable convective heat losses.

The single spike under the simulated conditions provided pressurized air at just below 800 °C at a thermal efficiency of about 80 %. 16.2 % of the absorbed heat is rejected in form of convective heat losses while 2.9 % of the absorbed heat are lost due to radiative heat losses. About 15 % of the total heat losses occur at the spike tip, while 85 % are lost via the cylindrical surface.

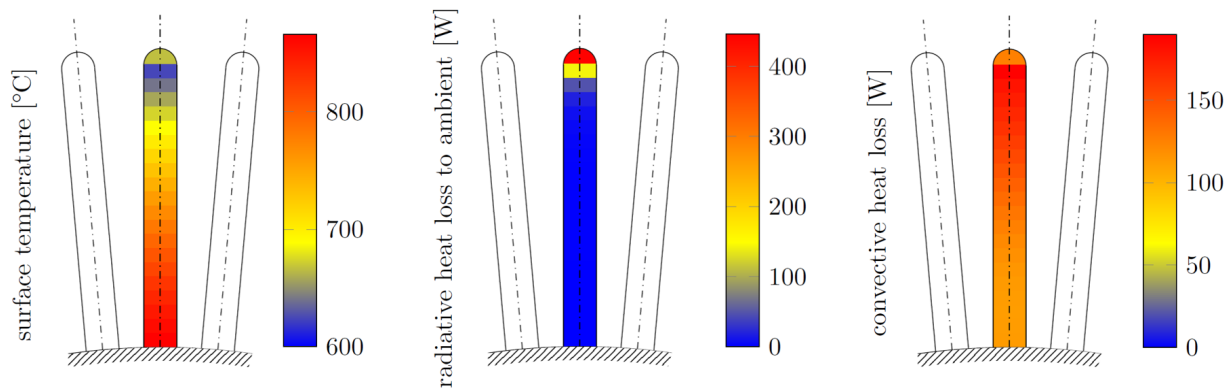


FIGURE 6: The surface temperature plotted along the spike (left) with radiative heat loss (centre) and convective heat loss (right)

CONCLUSION

An averaging assumption for jet impingement Nusselt numbers has been made based on a CFD analysis of a spike's tip region. The Nusselt number range achievable is sufficient to operate under a flux of 1.0 MW/m^2 .

The thermal efficiency of the spike under these conditions was calculated at about 80 %. The intended macro-volumetric effect seems to have been achieved with the highest surface temperatures occurring towards the root of the spike. It is noteworthy that only 2.9 % of the absorbed energy were lost due to radiative heat losses.

Heat transfer improvement in the spike tip region could see higher fluxes permissible before approaching material limitations. Further studies are required to identify tip geometries that provide heat transfer characteristics of the magnitude required while delivering a low pressure drop. The way wind may penetrate the geometry or be blocked thereby should be investigated as well as potential air velocities occurring due to updraft caused by natural convection.

A laboratory model is currently being designed to confirm the assumptions within the heat transfer modeling, including the jet impingement cooled tip region. With gathered and improved understanding the simulation model can be updated and initial performance optimization conducted.

ACKNOWLEDGEMENTS

The authors thank the late Prof. Detlev Kröger for all guidance and inspiration received. The authors further thank the Department of Mechanical and Mechatronic Engineering and the Solar Thermal Energy Research Group (STERG) at Stellenbosch University for funding of this research through the Eskom Chair in Concentrating Solar Power.

REFERENCES

- [1] M. Lubkoll, T. W. V. Backström, and D. G. Kröger, "Survey on Pressurized Air Receiver Development," in *2nd Southern African Solar Energy Conference 2014*, (Port Elizabeth, 2014).
- [2] M. Lubkoll, T. Von Backstroem, T. Harms, and D. G. Kröger, *Energy Procedia* **69**, 461–470 (2015).
- [3] D. G. Kröger, "Spiky Central Receiver Air Pre-heater (SCRAP)," Tech. Rep. (University of Stellenbosch, Stellenbosch, 2008).
- [4] N. Zuckerman and N. Lior, *Advances in Heat Transfer* **39**, 565–631 (2006).
- [5] M. Behnia, S. Parneix, and P. Durbin, Center Turbulence Research Annual Research Briefs 149–164 (1997).
- [6] Y. A. Cengel and A. J. Ghajar, *Heat and Mass Transfer: Fundamentals and Applications*, fourth ed. ed. (McGraw-Hill, Inc., New York, 2011).
- [7] O. Garbrecht, F. Al-Sibai, R. Kneer, and K. Wiegardt, "Numerical Investigation of a New Molten Salt Central Receiver Design," in *SolarPACES* (Marrakech, 2012).
- [8] J. R. Howell, "A Catalog of Radiation Heat Transfer Configuration Factors," Tech. Rep. (The University of Texas at Austin, Austin, 2011).